Hindawi
Shock and Vibration
Volume 2022, Article ID 6797938, 15 pages
https://doi.org/10.1155/2022/6797938

*Research Article*

# Analytical and Numerical Investigation of Knee Brace Equipped with a Shape Memory Alloy Damper

**Milad Shakiba and Seyed Mohammad Reza Mortazavi**

*Department of Civil Engineering, Shahid Rajaee Teacher Training University, Lavizan, Tehran, Iran*

Correspondence should be addressed to Seyed Mohammad Reza Mortazavi; mortazavi@sru.ac.ir

Received 13 May 2022; Revised 12 August 2022; Accepted 22 August 2022; Published 13 September 2022

Academic Editor: Cheng Fang



Shape memory alloys (SMAs) are some of the new materials that have attracted the attention of many engineers due to their unique behavior. The most important advantage of these materials is their superelastic behavior, which allows the alloy to return to its original shape after a large deformation. In superelastic behavior, the shape memory alloy can also dissipate a significant amount of energy while returning to its original shape. In this research, the superelastic alloy made of nitinol has been used to improve the performance of knee dampers. For this purpose, a frame equipped with a knee damper was selected as the reference model and was modelled in Abaqus numerical software and validated with an experimental model. After ensuring the correct behavior of the numerical model, the SMA damper was installed perpendicular to the knee damper, between the knee damper and the beam to column connection. In this paper, two parameters of the SMA damper cross section area and SMA length were investigated. Based on the observed results, increasing the length of SMA increases the system resistance. As the cross section area of the SMA damper increases, the effect of the SMA length on the resistance of the system increases. On the other hand, increasing the cross section area of the SMA significantly increases the recentering of the system. Due to the significant recentering that the SMA damper creates in the structure, the amount of energy dissipation of the system is reduced compared to the reference model. The amount of dissipated energy depends on the length and cross section area of the SMA damper. Thus, the longer the SMA, the greater the energy dissipation, and the lower the SMA cross section area, the lower the system energy dissipation.

## 1. Introduction

Due to the inevitability of earthquakes and their impacts, it is necessary to find an appropriate solution to control this natural phenomenon [1, 2]. A conservative approach to the design of civil engineering structures is very important in that uncertainty in structural properties and loads are calculated using safety factors [3, 4]. In general, the main task of a structure is to withstand the loads and transfer them to the foundation of the structure. The energy applied to the structure must be transferred to the ground or dissipated through a suitable mechanism. For this reason, it is necessary to apply different methods in the improvement of buildings according to the existing conditions [5–7]. Preventing structural collapse and saving lives is the most important criterion for the structural design of earthquake-resistant buildings. Severe structural damage, as well as widespread destruction of building performance after a major earthquake, can have an impact on the intensity of community welfare and resilience [8, 9]. Some buildings are left in an unusable state due to the inelastic behavior shown at excessive load levels. Repairing a severely damaged building is often economically impossible [10]. Therefore, it is useful to develop statically elastic structural systems with the capability of "self-centering" (i.e. returning to the initial geometric position after an earthquake) [11]. With this approach, the risk of structural failure can be reduced.

Some of the recent technological developments in the field of seismic-resistant steel structures are presented by Fang et al. that cover various aspects, such as emerging smart materials, novel members, and the innovative design of structural systems [12]. Engineers have introduced many

solutions to improve the behavior of a structure, but among these solutions, dampers are in a special place. Energy dissipation in a structure is usually achieved in the range of its nonlinear behavior, and the behavior of a damper is based on this phenomenon. Among the dampers, there is a knee damper that dissipates energy by plastic deformation [13, 14]. This element is attached to a brace, and this brace remains elastic during loading. Major nonlinear deformations and damage to the structure are concentrated in the knee [15]. Therefore, improving the behavior of this damper is very important. Compared to viscoelastic materials and metals with low yield strength, SMA dampers have advantages, such as fatigue-resistance ability, high damping capacity, high recoverable deformation, and stable behaviors [16, 17].

Shape memory alloys (SMAs) are one type of smart material with several special properties. In addition to the high driving force and intelligence, these materials have the properties of superelasticity and shape memory effect [18, 19]. These materials can eliminate large deformations and are resistant to corrosion and fatigue [20]. Due to these advantages, SMA materials are considered as a new material for structural engineering applications [21, 22]. To date, SMA materials have been widely used in the construction industry as bolts and structural shapes in steel buildings [23, 24] and SMA bars in reinforced concrete buildings [25, 26]. These materials are also implemented in SMA-based recentering dampers in bridges [27, 28]. Recently, a case study has been presented that demonstrates the application of SMA cable-restrained high-damping rubber (SMA-HDR) bearings in the Datianba $^{\#}2$ highway bridge, a real project that employs the proposed bearings for the first time in the world [29]. In addition to the above, SMA materials have been used in nonbuckling braces [30–32] and base isolators [33, 34].

SMA bracing system has been used in buildings to improve seismic performance. Self-centering brace systems have been developed for friction forces and energy dissipation using shape memory alloys (SMAs) [35]. The practical advantage of SMA is in its performance in creating resistance against structural systems under severe earthquakes [36]. Various studies have investigated the performance of SMA-based members and braced steel frames numerically and experimentally [37, 38]. Also, many studies have been conducted in the field of improving the nonlinear behavior of structures. Andrawes and DesRoches studied the potential application of a superelastic material in multispan reinforced concrete bridges and indicated the capability of SMA as a restrainer for bridges [39]. They also studied temperature effects on the performance of SMA restrainers [40]. Hui et al. presented a preliminary study on the evaluation of an innovative energy dissipation system with shape memory alloys (SMAs) for structural seismic protection [41]. Oliveira et al. evaluated the nonlinear dynamics behavior of one degree of freedom SMA oscillator indicating dynamical jumps as well as pseudoelastic behavior [42]. Mirzai and Attarnejad proposed a new superelastic damper and used the proposed damper in the EBF frame. They used time history analysis to investigate the SMA performance on the structure [43–46]. Aryan and Ghassemieh utilized this material in a multispan bridge and proposed an innovative superelastic system for retrofitting. They also suggested a new bridge design method that can simultaneously mitigate the effects of vertical and horizontal seismic excitations [47–49]. Abbass et al. used a new approach to rehabilitate the previously designed bridge. They divided the bridge into the three zones and utilized near-surface mounted SMA in a zone in which plastic deformation was more likely [50]. Farmani and Ghassemieh showed that SMA materials could be used as bolts and tendons in steel connections. In their numerical studies, the rate of permanent deformations decreased after unloading and fell almost to zero [51, 52].

Ghassemieh et al. evaluated the effectiveness of these materials on concrete shear walls. Their studies consisted of several solid and coupled shear walls to show that SMA could reduce the damage to the concrete in the walls, especially in the coupling beams [53–55]. Sadeghi and Hesami presented a finite-element analysis in which SMA was used as dowel bars on the jointed concrete pavements and used the fatigue-resistance property of SMA [56]. Alam et al. assessed the seismic fragility of a multispan continuous highway bridge using rubber bearings and SMA restrainer [57, 58]. Dezfuli and Alam used superelastic SMA wires in the bridge base isolation system to improve the seismic behavior of the structure. They showed that SMAs can considerably improve the seismic performance of piers by reducing the base shear [59, 60].

The knee bracing system has been investigated as a new structural system by researchers. Hsu et al. experimentally evaluated the performance of the knee-braced system by using cyclic loading [61]. Mofid and Khosravi conducted several types of research on the nonlinear behavior of the KBF system to predict approximately that behavior [62, 63]. Aniello and Landolfo studied the influence of using different knee bracings to improve the structural response of a frame through nonlinear dynamic analysis [64].

In this study, the effect of shape memory alloys on improving knee damper behavior is investigated. For this purpose, an experimental knee system is modelled and validated in Abaqus finite-element software, and SMA is placed in it with different lengths. The proposed systems are subjected to cyclic loading, and their behavior is compared with each other.

## 2. Shape Memory Alloys (SMAs)

Shape memory alloys are intelligent and innovative materials that, due to their unique behaviors, have found many and varied applications in various scientific, industrial, and even engineering fields in recent decades. The most important and obvious feature of these materials is recentering, which is due to the change of atomic phase in these alloys. This behavior causes the alloy to be able to withstand many deformations and return to its original shape, depending on the temperature conditions [20].

The SMAs have two atomic structures called austenite and martensite. The austenite state is stable at high temperatures and low stresses, while the martensite state is stable

at low temperatures and high stresses. By applying thermal and mechanical loads, these two phases can be converted to each other. In general, these structures require four characteristic temperatures to convert to each other. According to Figure 1, the characteristic temperatures are $A_s$, $A_f$, $M_s$, and $M_f$, which are the austenite start-up temperature, the austenite-end temperature, the martensite start-up temperature, and the martensitic end-temperature, respectively.

Superelastic behavior governs SMA as the temperature of alloy at zero stress is more than $A_f$. Thus, in the above-mentioned scenario, the atomic structure of SMA would be austenite, and it would be responsible for triggering the superelastic behavior. Figure 2 indicates the stress-strain curve of this behavior, corresponding to no permanent deformation remains in the alloy. This phenomenon occurs due to the atomic structure of austenite because this structure always tends to return to its original form. The atomic structure is constantly changing during the loading and unloading process. These changes are due to the instability of atomic structures at different temperatures and stresses. At the phase of superelastic behavioral, since the austenite atomic structure is not stable at high stresses, after imposing some more stress, the structure of alloy will be unstable and must become a stable structure at high stresses. Therefore, the atomic structure of austenite is converted to martensite at high stress, and during this conversion the stiffness decreases (point 1). After the transformation is completed, the entire alloy has a martensitic structure and the stiffness of the alloy increases (point 2). During the unloading, the amount of stress in SMA diminishes and due to the fact that the martensite atomic structure is not stable at low stresses, the SMA needs to alter the atomic structure of itself (point 3). At this moment, the alloy atomic structure alters its states to austenite (point 4). Hence, no permanent deformation is observed in the superelastic behavior martensite, and the amount of its dissipated energy is lower than that in any other behavioral states.

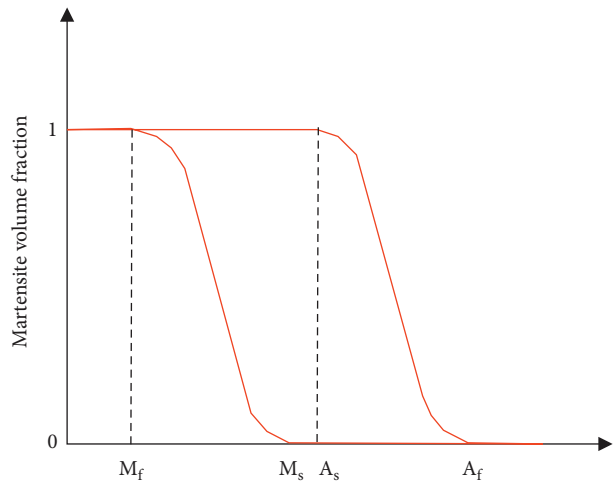


Figure 1: Change of martensite volume fraction with temperature.

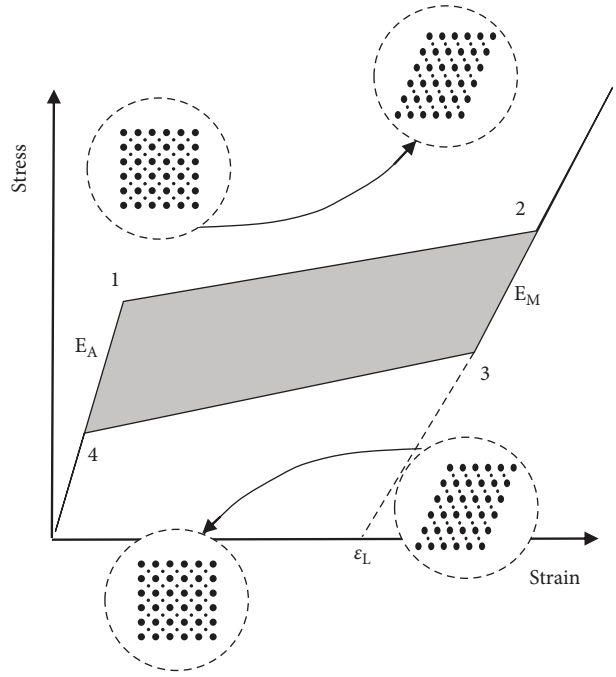


Figure 2: Stress-strain diagram of superelastic SMA [55].

## 3. Knee Dampers

In recent decades, many control systems have been tested to reduce the vibrations of structures due to dynamic forces. One of the effective methods in reducing the seismic response of the structure is the use of energy absorption systems. These systems perform special nonlinear behavior, which absorbs a large amount of energy entering the structure, as a result of which the amount of energy received by other structural members is reduced and thus a lower force will be generated in them.

Moment-resisting frames (MRF) and concentrically braced frames (CBF) are examples of traditional control systems to reduce the vibrations of structures. In the MRF system, lateral stiffness is limited to control deflections and in the CBF system, is stiff and their ductility is limited because of the buckling of the diagonal brace. The high ductility of MRF systems, which enables energy dissipation at a good level, and the significant stiffness of CBF systems, which limit drifts, are the main advantages of these systems [65]. On the other hand, the eccentrically braced frame (EBF) system was proposed by Roeder et al. to overcome the deficiencies of CBF and MRF [66]. In the EBF system, the brace member provides the stiffness of the frame and ductility is provided by connections with shear or flexural hinges. These components are formed on the end or middle of gravity loads bearing girders in the known configurations of the EBF system leading to uneconomically large sections for beam elements. However, researchers have been interested in the seismic performance of EBF and performed so many beneficial studies on this subject matter [67–69].

To address the problems of conventional bracing systems, Aristizabal-Ochoa introduced a new system called Disposable Knee Bracing Frame (DKBF) [70]. In this system, instead of connecting to the junction of the beam and the column, the end of the brace is connected to the knee element and the rigidity of the structure is provided by the

diagonal brace and its ductility and energy dissipation are provided by the knee element. In this system, buckling in the brace reduces energy dissipation potential. For this purpose, the brace is designed in such a way that it does not buckle. Hence, Balendra et al. introduced a system called the knee brace frame. In the new system provided by them, the diagonal brace does not buckle and, on the other hand, provides lateral stiffness to the frame. The knee element provides flexibility and energy dissipation by bending yield [15]. During large drifts, the knee element yields first, and the bracing behavior remains linear. Shear and flexural yielding mode and nonlinear behavior of the knee bracing under lateral loading were proposed by Mofid and Khosravi [62]. Their research showed that if the knee anchor and the inclined brace were parallel to the diagonal of the frame and the diagonal brace passed through the beam-column intersection, the structure could have maximum earthquake resistance. According to the studies, it is clear that knee bracing is effective in reducing parameters, such as the distribution of peak horizontal deflections, story shear, column bending moments, and beam ductility at a certain level of earthquake [65].

## 4. Studied Model

Balendra and his colleagues performed various full-scale tests on the knee brace frame system. The tests include different modes of bending and shear yielding in the knee brace. The tests also include the type of connection of the diagonal brace to the knee member and the type of knee sections used in the frame. They tested the knee model with flexural behavior under quasidynamic loading to investigate the nonlinear response of the frame [15]. Figure 3 shows the model tested by Balendra et al.

They selected the beam and column sections so that they remained almost elastic within the load range. The dimensions of the bracings were also chosen so that they not only remained elastic during loading but also did not buckle. Stiffeners with a thickness of 20 mm are installed at the connection of the beam to the column to prevent the buckling of the column web. At the joint of the knee to the beam and the column, stiffeners with similar thickness were used. These stiffeners are welded to beams and columns. Also, for easy knee replacement, 15 mm plates were used to connect the knee to the beam and column. In Table 1, the sections used in the mentioned system are presented. All elements of the structure are made of steel with a yield stress of 350 MPa, except for the knee part, where the steel used has a yield stress of 417 MPa. The elastic modulus and Poisson's ratio of the steel members are 190 GPa and 0.3, respectively. In Balendra et al.'s research, earthquake forces were simulated by a sinusoidal base excitation load. The excitation frequency was 20 rad/s. The initial amplitude of the excitation was 2.25 m/s$^2$, and this amount is increased by 0.79 m/s$^2$ after every five cycles.

## 5. Numerical Modelling

The FEM is a numerical method and solution for the physical problems, described with the differential equations.

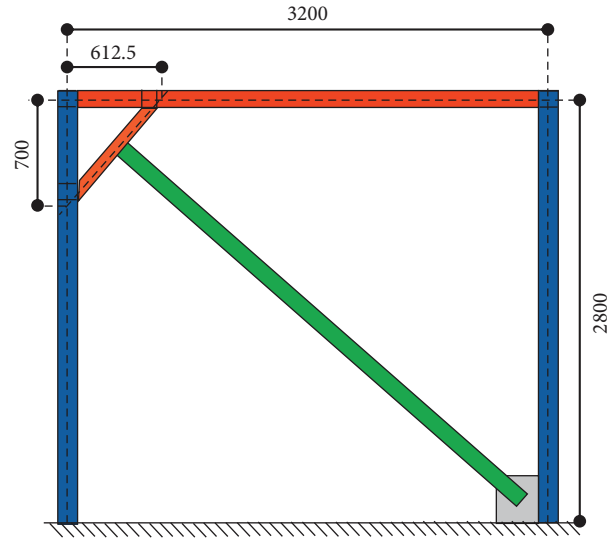


Figure 3: KBF system made by Balendra et al.

Table 1: Properties of sections used in the knee system.

| Element type | Section (mm) |
|---|---|
| Beam | WF $125 \times 125 \times 23.8$ |
| Column | WF $100 \times 100 \times 17.2$ |
| Brace | C-channels $100 \times 50 \times 5$ |
| Knee damper | SHS $60 \times 60 \times 4.5$ |

Because of Abaqus software ability to deal with a wide variety of static, quasidynamic, and dynamic analyses as well as its capability to take into account the nonlinear behavior due to large deformations, this software is used in simulating the studied system. Solid and shell elements have been used in modelling the components of the system, which are of the eight-node and four-node types, respectively. All components of the structure except the knee are modelled with shell elements. The knee link is modelled to accurately study the stresses, strains, and plastic behavior of solid elements, which are more accurate in calculations than the shell elements.

In this paper, the stress-strain behavior of steel materials is assumed to be bilinear, which includes the elastic zone and the postyield zone, and due to the loading cycles of the system, the kinematic behavior has been applied. Defining the interaction between all the components in contact with each other is one of the important points in modelling. To define the interaction between the components of the studied frame (considering that in modelling this system, a combination of solid and shell elements is used and on the other hand solid elements only have translational degrees of freedom and shell elements have degrees of rotational freedom additionally). All components of the frame, except the knee, are merged and the interaction at the knee contact with the beam, column, and brace is of the tie type, in which the relative motion of the element nodes is restricted in three transmission directions. In the studied frame, the dimensions of the mesh are considered to be about 50 mm in the areas far from the frame connected to the knee in which

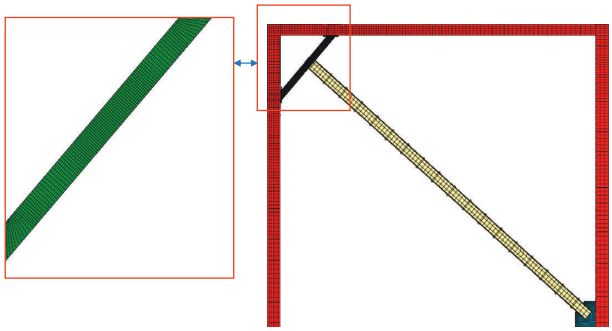

Figure 4: Numerical model meshing.

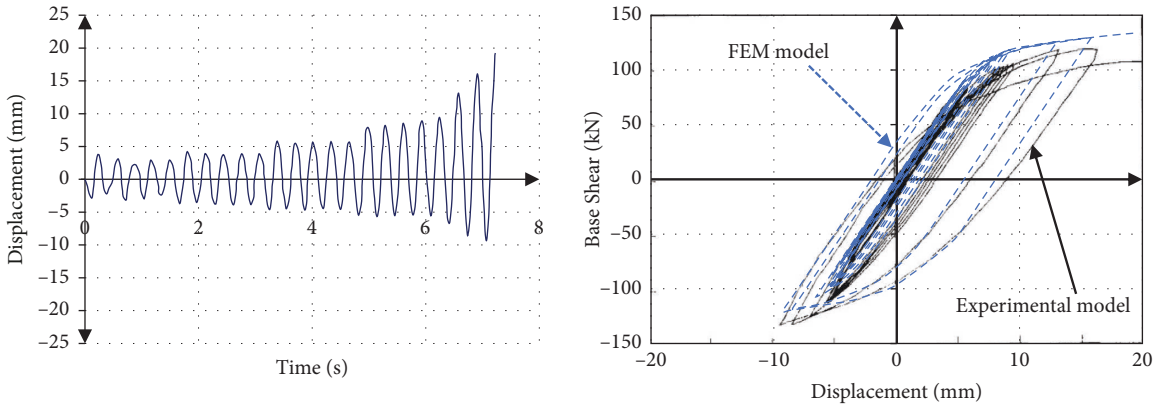


Figure 5: Comparison of the FEM model and the experimental system.

significant stress and plastic behavior are not formed. In the areas close to the knee connections, the mesh size decreases to about 20 mm; knee link mesh is considered from 6 to 10 mm. The details of the mesh are shown in Figure 4. As the dimensions of the meshes become larger in places where their behavior is linear, the dimensions of the stiffness matrix become smaller [71].

In order to apply the boundary conditions, the bottom of the columns is considered fixed and a cyclic load is applied to the top of the structure. Figure 5 shows the loading protocol and the results of the numerical and experimental models. By comparing the FEM results with the experimental results, it is shown that the FEM model can accurately predict the experimental results. To validate the accuracy of the model, the amount of energy dissipation in the experiment and FEM model is presented in Figure 6 for the last four cycles. The difference between these models is about 3% to 10%. Hence, the proposed FEM model has a relatively good match to the experimental. Figure 7 also shows the von Mises stress tensor, according to which most of the plastic deformation occurs in the knee.

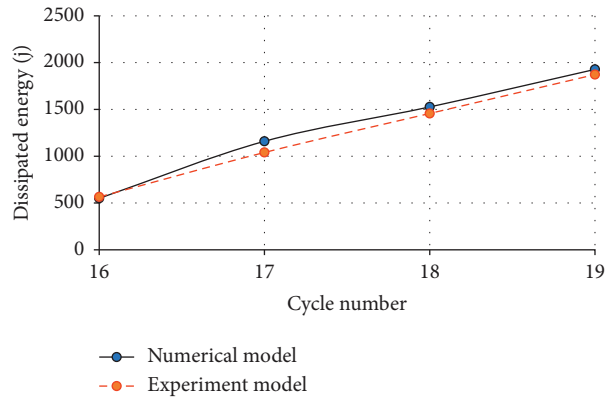


Figure 6: Energy dissipation at the last four cycles.

## 6. SMA Modelling

In order to model SMA behavior superelastically, the default option defined in Abaqus has been used. This default models the superelastic behavior and is suitable for alloys, such as nitinol. In this model, the structures of austenite and martensite are considered isotropic. The stiffness and Poisson's ratio of the alloy is calculated based on the amount of strain applied to the alloy and the rate at which atomic structures are converted to each other.

$$E = E_A + \xi(E_M - E_A), \tag{1}$$

$$\upsilon = \upsilon_A + \xi(\upsilon_M - \upsilon_A). \tag{2}$$

In (1) and (2), $\xi$ stands for the martensite fraction, $E_A$ and $E_M$, respectively, represent austenite and martensite Young's modulus. Moreover, $\nu_A$ and $\nu_M$ indicate the austenite and martensite Poisson's ratio, respectively. After certain stress, austenite is entirely transformed into martensite. In these

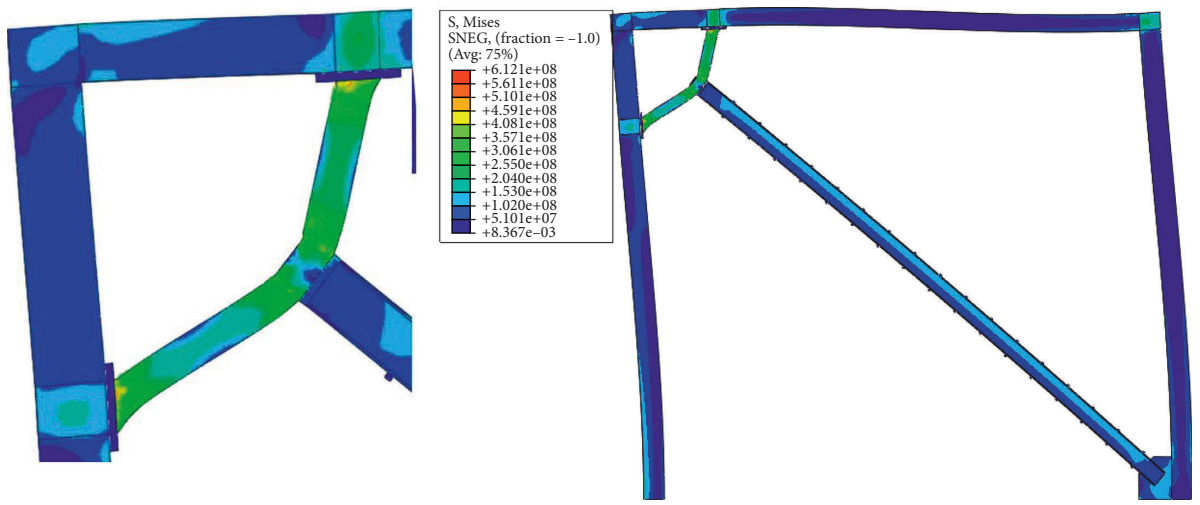


Figure 7: Von Mises stress contour in the numerical model.

Table 2: Superelastic SMA physical and mechanical properties [72].

| Diameter (mm) | Length (mm) | $A_s$ (°C) | $E_A$ (GPa) | $\sigma_{Ms}$ (MPa) | $\sigma_{Mf}$ (MPa) | $\sigma_{As}$ (MPa) | $\sigma_{Af}$ (MPa) | Temperature (°C) |
|---|---|---|---|---|---|---|---|---|
| 1.8 | 152 | −26 | 40 | 538 | 573 | 104 | 69 | 21 |

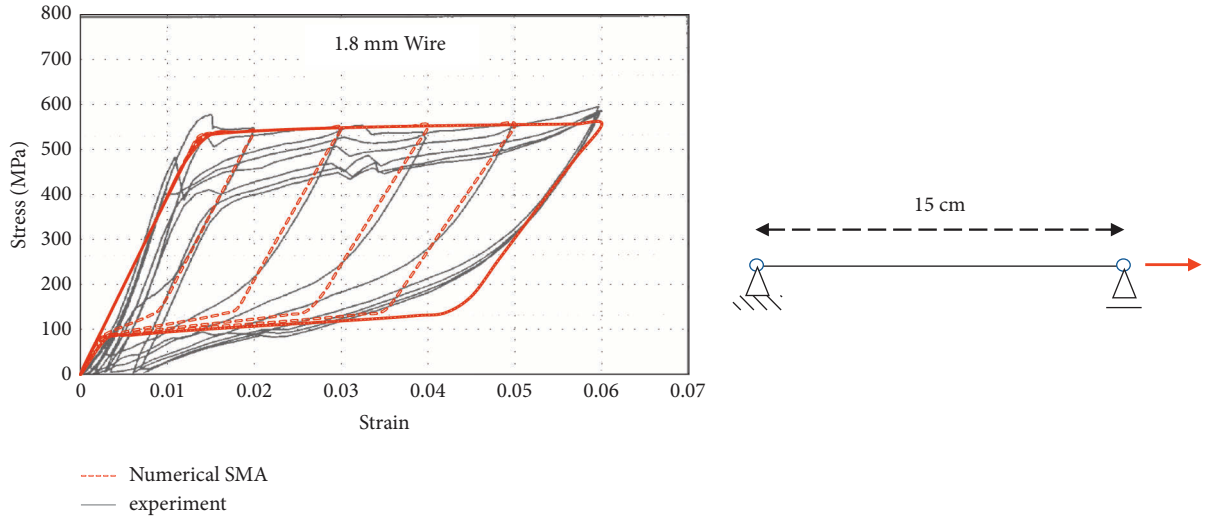


Figure 8: Validation of numerical wire model made of shape memory alloy.

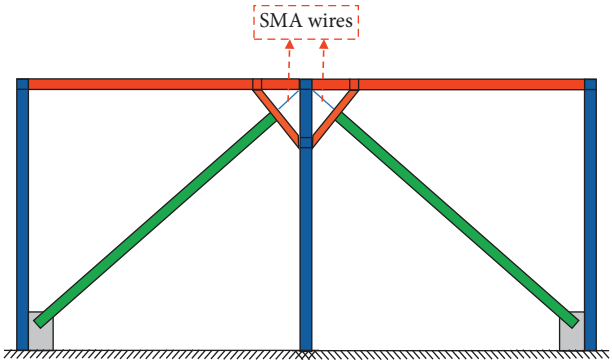


Figure 9: Location of SMA damper in the knee system.

Table 3: Properties of the studied numerical models.

| | Knee section dimension (mm) | | | Number of SMA wires | Length of SMA wire (mm) |
|---|---|---|---|---|---|
| | Width | Height | Thickness | | |
| KBF | 60 | 60 | 4.5 | — | — |
| KBF-10-1 | 55 | 55 | 4 | 2 × 20 D1.8 mm | 100 |
| KBF-10-2 | 55 | 55 | 3.5 | 2 × 26 D1.8 mm | 100 |
| KBF-10-3 | 50 | 50 | 3 | 2 × 40 D1.8 mm | 100 |
| KBF-10-4 | 50 | 50 | 2.5 | 2 × 44 D1.8 mm | 100 |
| KBF-15-1 | 55 | 55 | 4 | 2 × 30 D1.8 mm | 150 |
| KBF-15-2 | 55 | 55 | 3.5 | 2 × 40 D1.8 mm | 150 |
| KBF-15-3 | 50 | 50 | 3 | 2 × 60 D1.8 mm | 150 |
| KBF-15-4 | 50 | 50 | 2.5 | 2 × 66 D1.8 mm | 150 |
| KBF-20-1 | 55 | 55 | 4 | 2 × 39 D1.8 mm | 200 |
| KBF-20-2 | 55 | 55 | 3.5 | 2 × 52 D1.8 mm | 200 |
| KBF-20-3 | 50 | 50 | 3 | 2 × 78 D1.8 mm | 200 |
| KBF-20-4 | 50 | 50 | 2.5 | 2 × 86 D1.8 mm | 200 |

relations, $\xi$ is between 0 and 1. If the structure of the alloy is completely austenite, it is equal to zero, and if the structure of the alloy is completely martensite, the value is 1.

In this study, nitinol wires have been employed in order to inspect the impact of superelastic damping on the behavior of knee dampers. A 15 cm long wire with diameter of 1.8 mm is subjected to cyclic loading. The nitinol alloy mechanical properties are given in Table 2. A two-node truss element is employed to simulate the SMA wire. Figure 8 shows the modelled wire and its cyclic response.

In this paper, in order to investigate the effect of SMA on the KBF system, the location of the SMA wire perpendicular to the knee is considered. According to Figure 9, the SMA wire is placed between the knee damper and the beam to column connection point. The most deformation occurs at this location, and since the SMA damper needs to be relocated to dissipate energy, this location was considered the SMA embedding location. The greater the deformation applied to the SMA, the greater its effect on the behavior of the structure. Because the SMA damper is considered a wire and these wires buckle under compressive stress, compression is not defined in the modelling of SMA behavior. To create this behavior in the modelling, in the property's module, in the definition of the elastic characteristics, the term "no compression" was ticked. By activating this expression, the stiffness of SMA becomes zero in the compressive range, and by this process, the buckling behavior of SMA wire is simulated. In order to consider the effect of SMA in cyclic loading in both positive and negative directions, two KBF systems were used as shown in Figure 9. In this system, if the SMA wire is buckled on one side, it will be stretched in the other direction and the buckling is compensated.

In this study, the length and number of SMA wires (stiffness) are investigated as two main parameters. In models equipped with SMA, the knee dimensions are smaller than the main model (model without SMA). These dimensions are chosen so that the stiffness of the numerical models is approximately equal to each other. Table 3 presents the properties of the studied numerical models. In name, the KBF model is without SMA and the number after it is the length of the SMA wires in centimetres.

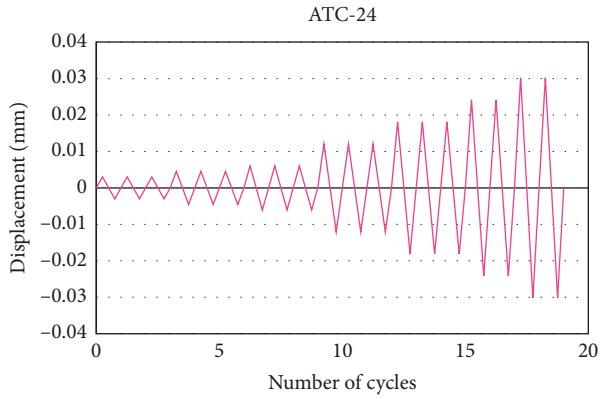


Figure 10: ATC-24 loading protocol.

Numbers 1 to 4 express the contribution of SMA to the stiffness of the model. Thus, number 1 indicates the lowest number of SMA wires and number 4 indicates the highest number of SMA wires.

Since the large deformation is not significantly applied to the structure in the loading presented in the Balendra model, the ATC-24 loading protocol according to Figure 10 was used to investigate the nonlinear behavior of numerical models, which was developed in the US to evaluate the seismic performance of steel structures elements [73].

This protocol includes 7 drifts; the first five drifts are repeated three times and the last two drifts are repeated two times. Usually, in large drifts with fewer repetitions, significant damage is done to the structure [74]. Figures 11–13 show the hysteresis diagrams for models equipped with ten, fifteen, and twenty cm SMA dampers. According to these figures, two parameters of cross-sectional dimension and the length of the SMA have a considerable impact on parameters, such as yield strength, permanent deformation, energy dissipation, and so on. In this study, the mentioned parameters are investigated separately and the effect of SMA in each of the models in comparison with the KBF model is presented. Accordingly, superelastic dampers have caused recentering in the structure, but the degree of the recentering varies depending on the length and stiffness of the SMA. In

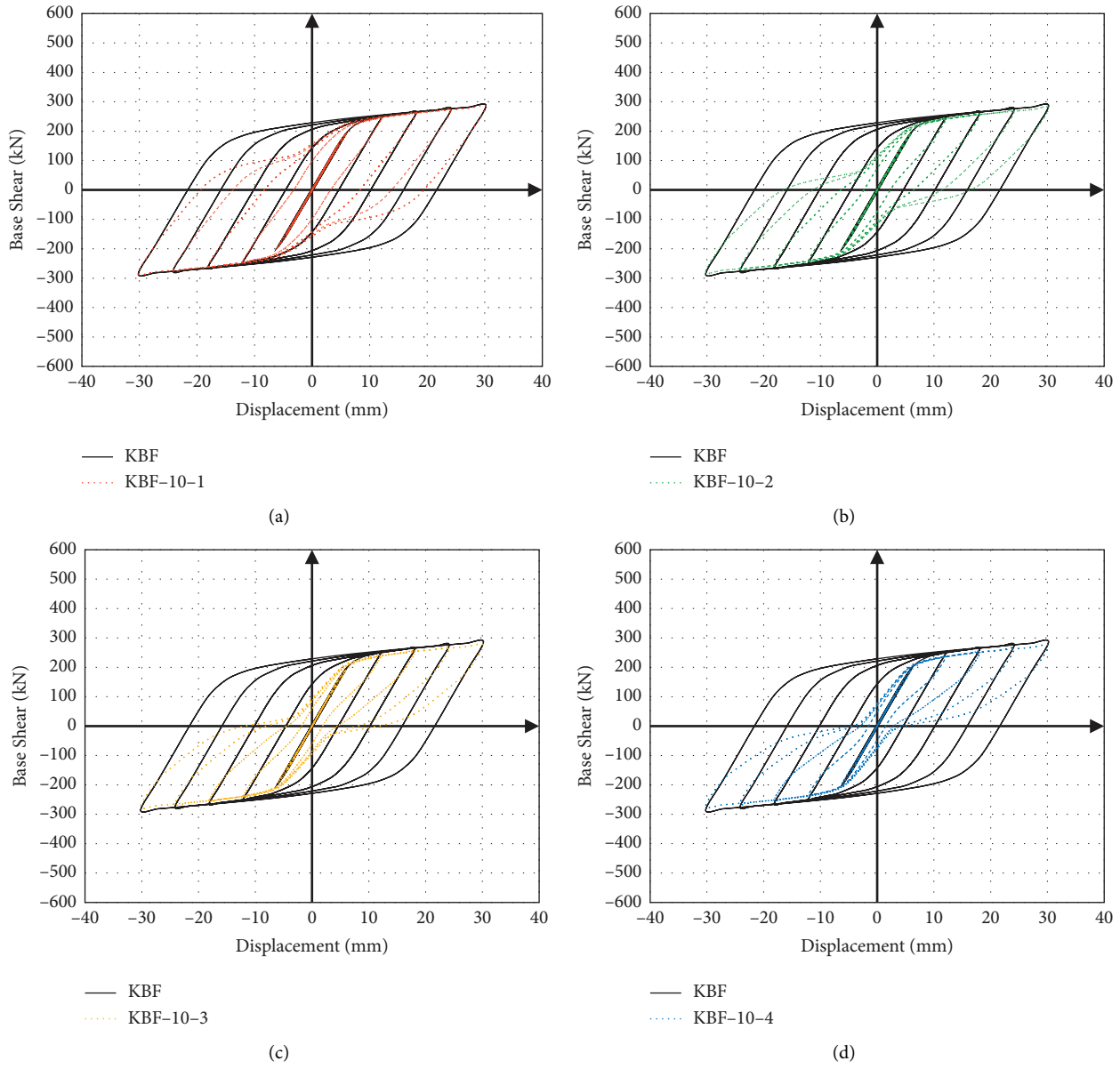


Figure 11: Hysterics curves of numerical models equipped with the SMA damper with a length of 100 mm.

none of the models, the permanent deformation is equal to zero and complete recentering has not occurred in the models. Complete recentering occurs in a structure equipped with SMA when all nonlinear deformation of the structure occurs in the SMA and the rest of the structural components are in the linear range. However, in the studied structures, a significant part of the nonlinear deformation occurred in the knee and therefore the recentering in the system is not complete.

## 7. Permanent Deformation

The ability of a structure for recentering depends on the degree of its permanent deformation. Thus, the less permanent deformation of the system is, the closer the hysteresis curve is to the flag. The maximum drift applied to the studied structure is around 1.2%, and at the maximum drift. In the maximum drift, the SMA strain is around 2.0%. Therefore, the SMA can use its maximum recentering capacity to return to the original shape. In the studied numerical models, the amount of permanent deformation is different and depends on the stiffness and length values of SMA. According to the hysteresis diagrams, it can be seen that the rate of recentering in the models in which the length of SMA is 10 cm is higher than that in the other models. Figure 14 shows the amount of permanent deformation for the studied structures where the negative and positive numbers indicate the permanent deformation in the negative and positive directions of loading, respectively. According to this figure, as the SMA stiffness increases, the rate of permanent deformation decreases. On the other hand, permanent deformation is directly related to SMA

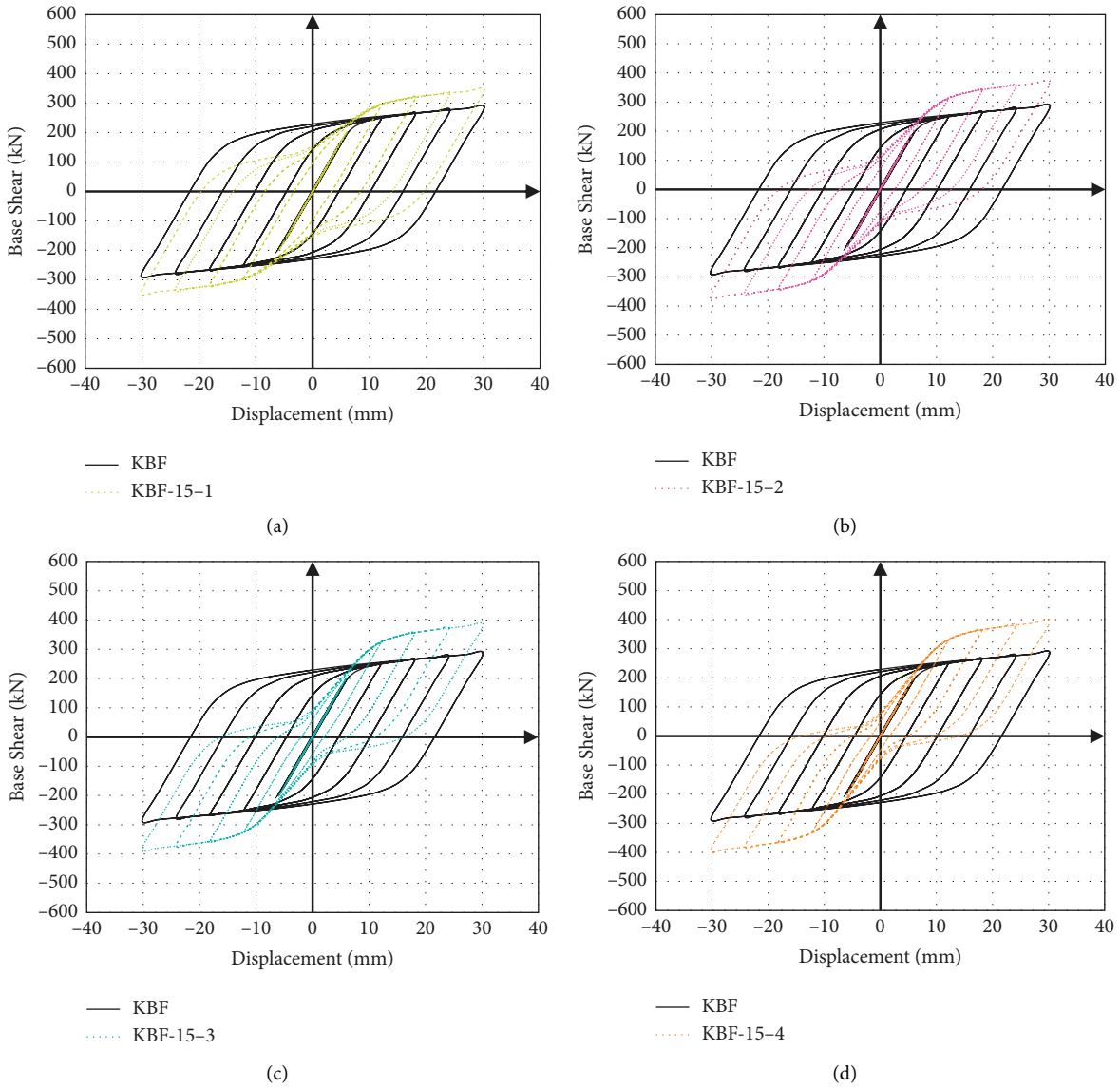


Figure 12: Hysterics diagrams of numerical models equipped with the SMA damper with a length of 150 mm.

length, so with the increases of the SMA length, the permanent deformation decreases. Accordingly, the KBF-10-4 model shows the least permanent deformation. According to Figure 14, with increasing stiffness in all models, the permanent deformation diminishes. However, the reduction value is not the same in different models. In models equipped with 20 cm SMA, it is observed that increasing stiffness has little effect on reducing permanent deformation. However, in models with SMA length of 10 cm, the increase in stiffness has a significant effect on permanent deformation. Therefore, the shorter the length of SMA, the higher the influence of stiffness on reducing permanent deformation.

## 8. Strength and Displacement

Strength and yield displacement are one of the most important parameters that have a great impact on the behavior of the structure. These two parameters also depend on the length and stiffness of the SMA. The dimensions of the knee and the cross section of the SMA are chosen so that the stiffness is almost equal in all models, and on the other hand, the stiffness of the SMA and knee wires are almost parallel. As the length of SMA increases, so does the value of yield displacement. Therefore, because the SMA and knee wires are parallel, as the length of the SMA increases, the rate of the yield displacement of the system (knee next to the SMA) increases. On the other hand, because the stiffness of the models is equal to each other, the strength of the structure also increases with increasing the yield displacement. Therefore, in the models in which the SMA length is considered to be 20 cm, more lateral strength is observed. Figure 15 shows the yield deformation and lateral strength for numerical models. According to this figure, models equipped with 10 cm SMAs have the least yield displacement and strength, and in 20 cm SMA models, these figures are higher than other models.

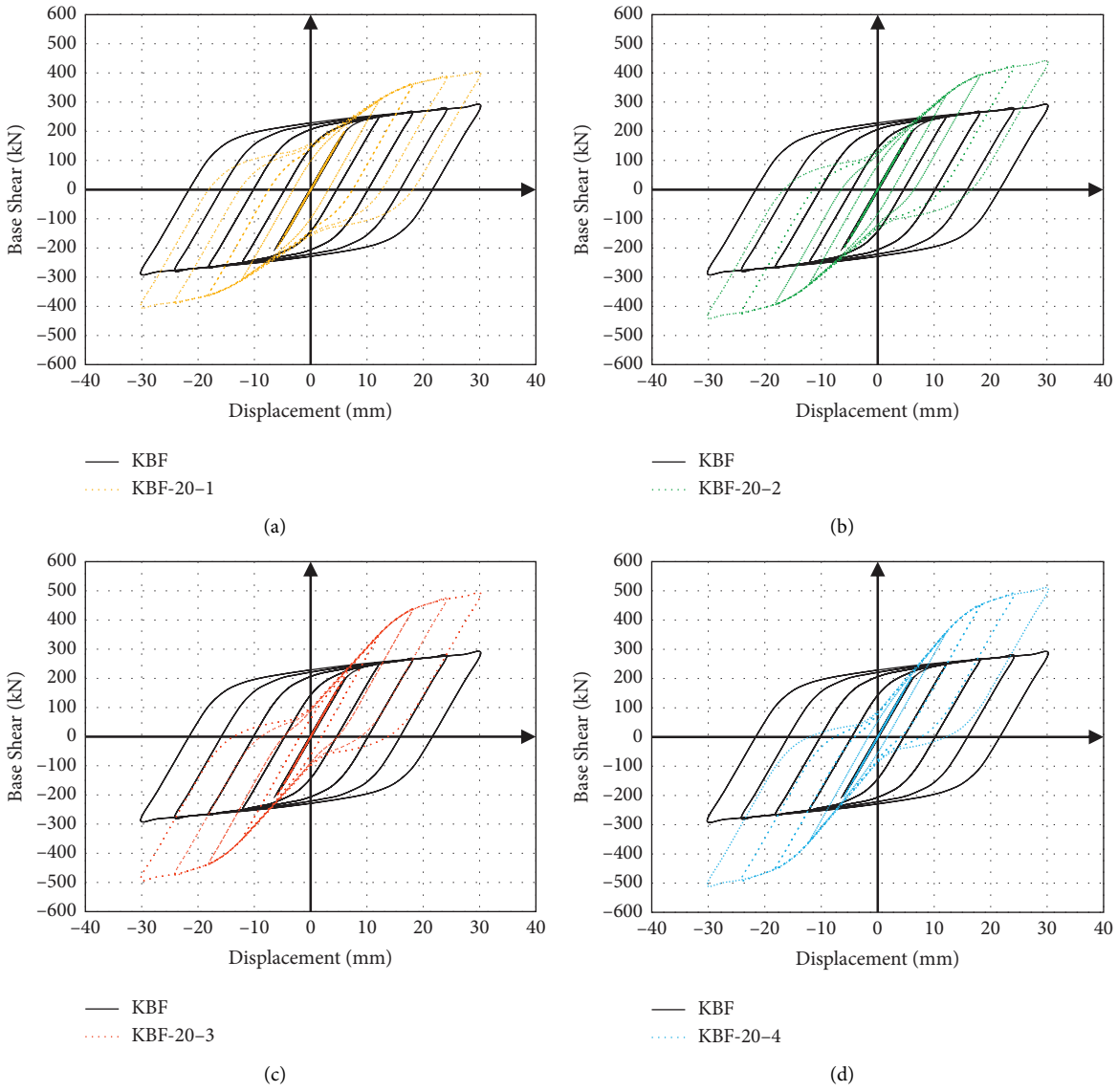


Figure 13: Hysterics curves of numerical models equipped with the SMA damper with a length of 200 mm.

Increasing the SMA's share of stiffness can increase the yield strength and displacement to some extent. However, in models equipped with a 20 cm long SMAs, this increase is more noticeable. Therefore, in the KBF-20-4 model, the highest strength and displacement of yield are observed. Although the effect of increasing stiffness on permanent deformation was very tangible in models equipped with 10 cm SMA, in these models, increasing stiffness has little effect on the yield strength of the model. However, in models equipped with a 20 cm long SMA, although the effect of increasing SMA stiffness has a small impact on the amount of permanent deformation, it has a significant effect on the yield strength.

## 9. Energy Dissipation

Regarding the type of damper, dissipation of energy happens through deformation and velocity. In viscous dampers, the dissipation of energy relies on velocity value, but in the conventional dampers, the dissipated energy relies on nonlinear deformation. The proposed dampers herein are of the latter, so those need nonlinear deformations in order to have energy dissipation. Since Figures 11–13 show the hysteresis diagrams of these dampers according to nonlinear displacement, the amount of energy dissipation can be found by calculating the area within each load cycle. Figure 16 shows the energy dissipation for load cycles. In the initial cycles, the behavior of the structure is almost linear, so the value of the dissipated energy in small cycles is negligible. Therefore, cycle No. 10 is presented in Figure 16. The amount of energy dissipation is directly related to lateral strength and permanent deformation. Therefore, in models where more permanent deformation and more strength are observed, there is more dissipated energy. According to the hysteresis diagrams, SMA dampers reduce the

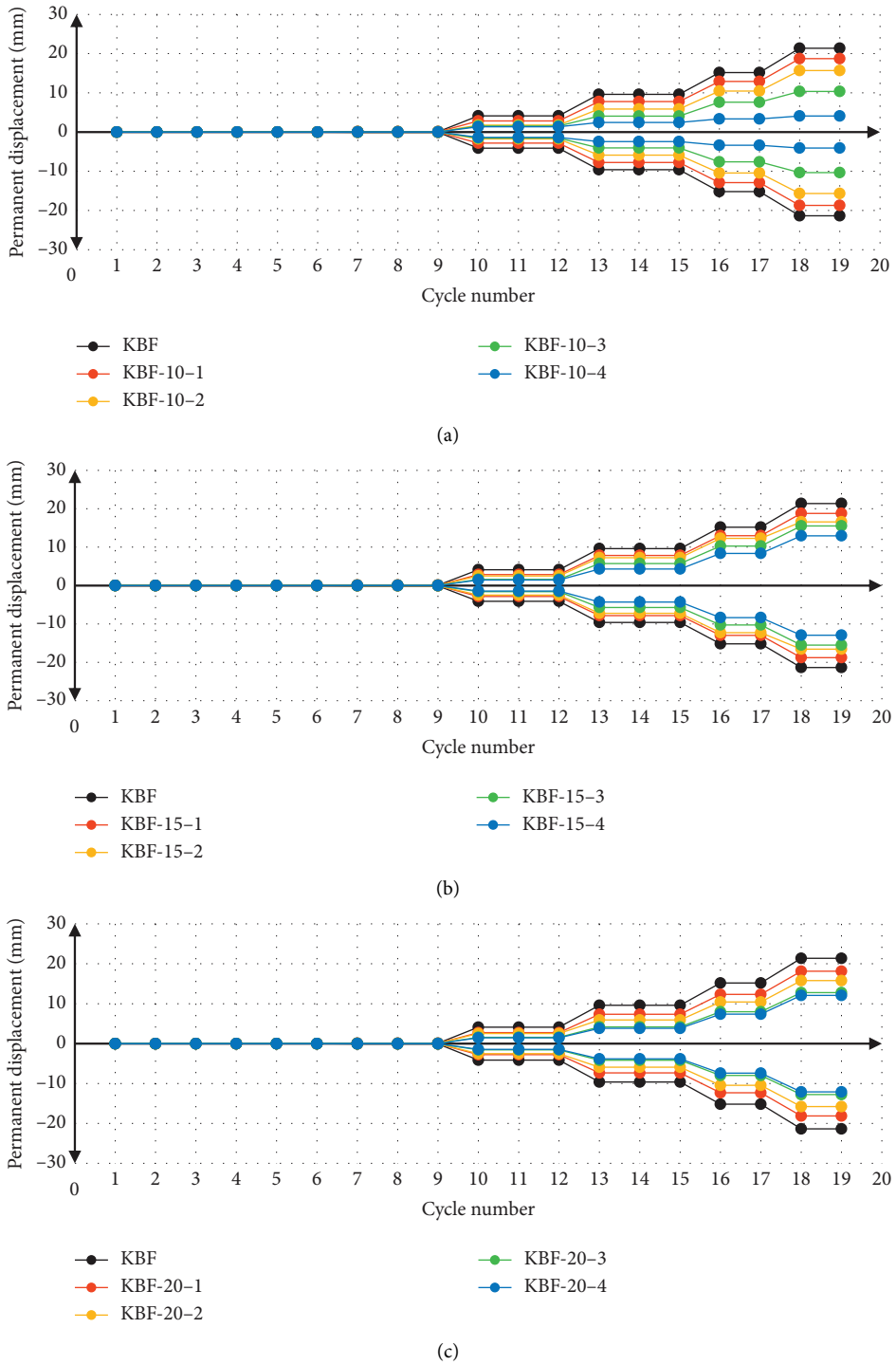


Figure 14: The amount of permanent deformation during the cyclic loading.

permanent deformation of the structure, and as a result, this reduces the energy dissipation capacity in the structure. On the other hand, in some models (systems equipped with 20 cm SMAs), the strength increases, and this increased the energy dissipation in the structure. Therefore, SMA dampers, on the one hand, reduce energy dissipation due to permanent deformation and, on the other hand, increase energy dissipation by increasing strength. As shown in Figure 16, the effect of recentering is greater than the increase in strength, because in all models the energy dissipation is less than the KBF reference model. But the energy dissipation levels in all models are different from the reference model. In models equipped with a 20 cm long SMAs, due to high strength and low recentering, the amount of energy dissipation is close to the reference model (KBF). Therefore, due to the increase in the length of the SMA damper, the amount of energy dissipation increases. Because

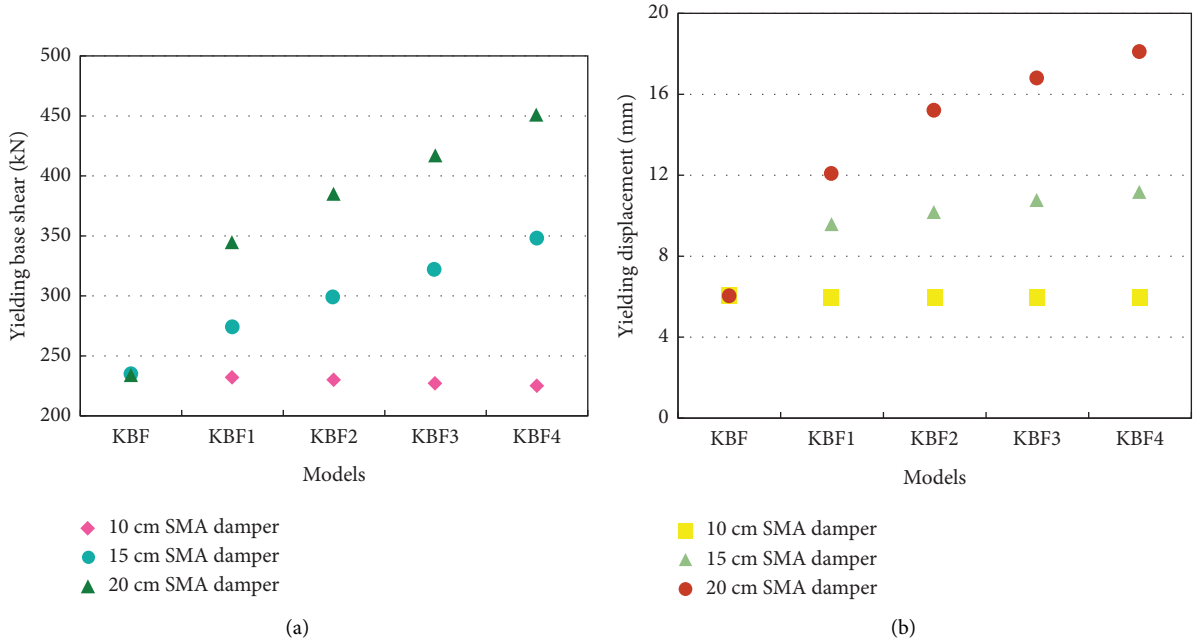


Figure 15: Yielding base shear and yielding displacement during the cyclic loading.

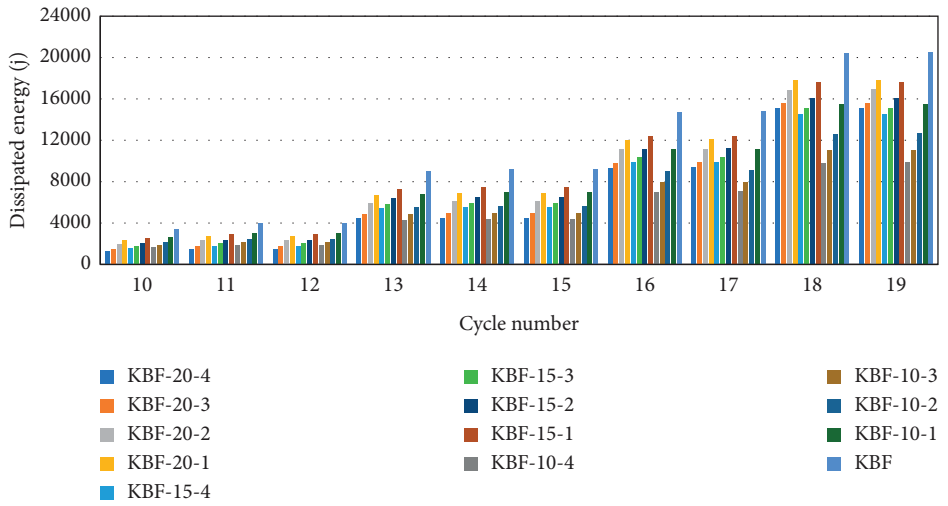


Figure 16: The amount of energy dissipation in 10 end cycles.

increasing the SMA length has increased the lateral strength of the system. For example, the energy dissipation for KBF-20-1, KBF-15-1, and KBF-10-1 models, the energy dissipation in the nineteenth cycle is 17860, 17640, and 15540 joules, respectively. Increasing the SMA damper stiffness has an inverse influence on the energy dissipation because with increasing the stiffness of the SMA damper, the degree of recentering increases and the energy dissipation decreases. For example, the energy dissipation in the nineteenth cycle for KBF-20-1, KBF-20-2, KBF-20-3, and KBF-20-4 is 17860, 16929, 15609, and 15112 joules, respectively.

## 10. Conclusion

This article aimed to study the impact of using SMAs on the improvement of knee damper behavior. For this purpose, a laboratory model was selected and validated under numerical modelling. Twelve models were subjected to cyclic loading and the effect of two parameters, namely, SMA damper length and stiffness on permanent deformation, yield strength, and energy dissipation, was investigated. Based on the numerical investigation, the following conclusions can be drawn:

(i) In the studied numerical models, the amount of permanent deformation is different and depends on the length and stiffness of SMA. According to the hysteresis diagrams, it can be seen that the rate of recentering in models with SMA length of 10 cm is higher than that in the other models. On the other hand, permanent deformation is directly related to

SMA length, so as the length of SMA increases, so does the rate of permanent deformation. Accordingly, in models equipped with SMA with a length of 10 cm, the least permanent deformation is observed. In models equipped with a 20 cm long SMA, it is observed that increasing stiffness has little effect on reducing permanent deformation.

(ii) Strength and yield displacement are important parameters that have a great impact on the behavior of the structure. These two parameters also depend on the length and stiffness of the SMA. According to the results, in models where the length of SMA is considered 20 cm, more lateral strength is observed and in models equipped with 10 cm, SMAs have the minimum yield displacement and strength. Increasing the SMA's share of stiffness can significantly increase yield strength and displacement. However, in models equipped with a 20 cm long SMAs, this increase is more noticeable. However, in models equipped with 10 cm long SMA, the effect of increasing stiffness on permanent deformation was very tangible, but in these models, increasing stiffness has little effect on the yield strength of the model. Therefore, SMA length is directly related to increasing structural strength.

(iii) The amount of energy dissipation is directly related to lateral strength and permanent deformation. According to the hysteresis diagrams, SMA dampers reduce the permanent deformation of the structure and this reduces the capacity of energy dissipation in the structure. But on the other hand, in some models, SMA dampers increase the strength and, as a result, increase the energy dissipation capacity in the structure. Therefore, SMA dampers, on the one hand, reduce energy dissipation capacity due to permanent deformation and, on the other hand, increase energy dissipation capacity due to increasing strength.

(iv) According to the results, the effect of recentering is greater than the increase of strength, because in all models the capacity of energy dissipation is less than the reference model. In models equipped with 20 cm SMAs, due to high strength and low recentering, the energy dissipation value is higher than that in the other models. Therefore, due to the increase in the length of the SMA damper, the amount of energy dissipation capacity increases. Increasing the stiffness of the SMA damper has an inverse effect on the energy dissipation capacity because with increasing the stiffness of the SMA damper, the degree of recentering increases and the energy dissipation capacity decreases.

## Data Availability

The data used to support the findings of this study are available from the corresponding author upon request.

## Conflicts of Interest

The authors declare that there are no conflicts of interest.

## Authors' Contributions

Milad Shakiba investigated the study, performed formal analysis, reviewed and edited the manuscript, conceptualized the study, validated the study, and proposed the methodology. Seyed Mohammad Reza Mortazavi was responsible for project administration, supervised the study, provided the resources, wrote the original draft, validated the study, conceptualized the study, and proposed the methodology.

## References

[1] M. Esfahani, M. Hoseinzade, M. Shakiba, F. Arbab, M. Yekrangnia, and G. Pachideh, "Experimental investigation of residual flexural capacity of damaged reinforced concrete beams exposed to elevated temperatures," *Engineering Structures*, vol. 240, Article ID 112388, 2021.

[2] M. Hoseinzade, M. Esfahani, F. Arbab, M. Shakiba, and M. Yekrangnia, "Residual flexural capacity of pre-cracked RC beams exposed to chloride penetration at the sea surface temperature," *Construction and Building Materials*, vol. 343, Article ID 128126, 2022.

[3] S. M. R. Mortazavi, M. Shakiba, and B. Zaeimdar, "Material effects on tangent modulus of steel square hollow section," *Journal of Rehabilitation in Civil Engineering*, vol. 11, no. 2, pp. 1–17, 2022.

[4] S. M. R. Mortazavi and M. Shakiba, "Experimental study on RC deep beams with non-prestressed tendons as main reinforcement," *Journal of Rehabilitation in Civil Engineering*, vol. 11, no. 1, pp. 43–59, 2023.

[5] M. Shekarchi and A. Khaloo, "Shear and flexural strengthening of steel beams with thick carbon fiber reinforced polymer laminate," *Journal of Rehabilitation in Civil Engineering*, vol. 9, no. 4, pp. 148–170, 2021.

[6] M. Shakiba, A. V. Oskouei, M. Karamloo, and A. Doostmohamadi, "Effect of mat anchorage on flexural bonding strength between concrete and sand coated GFRP bars," *Composite Structures*, vol. 273, Article ID 114339, 2021.

[7] A. Doostmohamadi, M. Karamloo, A. Vatani Oskouei, M. Shakiba, and A. Kheyroddin, "Enhancement of punching strength in GFRP reinforced single footings by means of handmade GFRP shear bands," *Engineering Structures*, vol. 262, Article ID 114349, 2022.

[8] N. Rajabpour, H. Naderpour, and P. Fakharian, "Evaluation of seismic resilience of urban infrastructure," *International Journal of Concrete Structures and Materials*, vol. 2, no. 1, pp. 77–87, 2017.

[9] N. M. Mirzai, H. M. Cho, and J. W. Hu, "Experimental study of new axial recentering dampers equipped with shape memory alloy plates," *Structural Control and Health Monitoring*, vol. 28, no. 3, Article ID e2680, 2021.

[10] N. M. Mirzai, I. Mansouri, J. Tezcan, P. O. Awoyera, and J. Wan Hu, "Estimating optimum parameters of a new SMA damper under different earthquake ground motions," *Structures*, vol. 33, pp. 2700–2712, 2021.

[11] D. J. Miller, *Development and experimental validation of self-centering buckling-restrained braces with shape memory alloy*,

The University of Illinois at Urbana-Champaign, Champaign, IL, USA, 2011.

[12] C. Fang, W. Wang, C. Qiu, S. Hu, G. A. MacRae, and M. R. Eatherton, "Seismic resilient steel structures: a review of research, practice, challenges and opportunities," *Journal of Constructional Steel Research*, vol. 191, Article ID 107172, 2022.

[13] S. Honma, K. Ebato, and Y. Harada, "Ductile steel knee brace with built-in comb-shaped seismic damper," *Journal of Constructional Steel Research*, vol. 184, Article ID 106765, 2021.

[14] T. Munkhunur, H. Tagawa, and X. Chen, "Steel rigid beam-to-column connections strengthened by buckling-restrained knee braces using round steel core bar dampers," *Engineering Structures*, vol. 250, Article ID 113431, 2022.

[15] T. Balendra, M. T. Sam, and C. Y. Liaw, "Diagonal brace with ductile knee anchor for aseismic steel frame," *Earthquake Engineering & Structural Dynamics*, vol. 19, no. 6, pp. 847–858, 1990.

[16] M. Dolce, D. Cardone, and R. Marnetto, "Implementation and testing of passive control devices based on shape memory alloys," *Earthquake Engineering & Structural Dynamics*, vol. 29, no. 7, pp. 945–968, 2000.

[17] X.-B. Zuo, A.-Q. Li, W. Sun, and X.-H. Sun, "Optimal design of shape memory alloy damper for cable vibration control," *Journal of Vibration and Control*, vol. 15, no. 6, pp. 897–921, 2009.

[18] F. Mücklich and H. Janocha, "Smart materials-the "IQ" of materials in systems," *International Journal of Materials Research*, vol. 87, no. 5, pp. 357–364, 1996.

[19] D. Z. Yang, *Smart Material and Smart System*, Tianjin University Press Tianjin, Tianjin, China, 2000.

[20] M. Rezapour, M. Ghassemieh, M. Motavalli, and M. Shahverdi, "Numerical modeling of unreinforced masonry walls strengthened with Fe-based shape memory alloy strips," *Materials*, vol. 14, no. 11, p. 2961, 2021.

[21] B. Wang and S. Zhu, "Cyclic tension–compression behavior of superelastic shape memory alloy bars with buckling-restrained devices," *Construction and Building Materials*, vol. 186, pp. 103–113, 2018.

[22] E. Abraik, S. F. El-Fitiany, and M. A. Youssef, "Seismic performance of concrete core walls reinforced with shape memory alloy bars," *Structures*, vol. 27, pp. 1479–1489, 2020.

[23] B. Wang, H. Jiang, and J. Wang, "Numerical simulation and behavior insights of steel columns with SMA bolts towards earthquake resilience," *Journal of Constructional Steel Research*, vol. 161, pp. 285–295, 2019.

[24] B. Wang, S. Zhu, K. Chen, and J. Huang, "Development of superelastic SMA angles as seismic-resistant self-centering devices," *Engineering Structures*, vol. 218, Article ID 110836, 2020.

[25] M. A. Youssef, M. S. Alam, and M. Nehdi, "Experimental investigation on the seismic behavior of beam-column joints reinforced with superelastic shape memory alloys," *Journal of Earthquake Engineering*, vol. 12, no. 7, pp. 1205–1222, 2008.

[26] B. Wang and S. Zhu, "Superelastic SMA U-shaped dampers with self-centering functions," *Smart Materials and Structures*, vol. 27, no. 5, Article ID 055003, 2018.

[27] A. H. M. M. Billah and M. S. Alam, "Performance-based seismic design of shape memory alloy–reinforced concrete bridge piers. I: development of performance-based damage states," *Journal of Structural Engineering*, vol. 142, no. 12, Article ID 4016140, 2016.

[28] A. H. M. M. Billah and M. Shahria Alam, "Performance-based seismic design of shape memory alloy–reinforced concrete bridge piers. II: Methodology and design example," *Journal of Structural Engineering*, vol. 142, no. 12, Article ID 4016141, 2016.

[29] C. Fang, D. Liang, Y. Zheng, and S. Lu, "Seismic performance of bridges with novel SMA cable-restrained high damping rubber bearings against near fault ground motions," *Earthquake Engineering & Structural Dynamics*, vol. 51, no. 1, pp. 44–65, 2022.

[30] D. J. Miller, L. A. Fahnestock, and M. R. Eatherton, "Development and experimental validation of a nickel–titanium shape memory alloy self-centering buckling-restrained brace," *Engineering Structures*, vol. 40, pp. 288–298, 2012.

[31] S. Moradi, M. S. Alam, and B. Asgarian, "Incremental dynamic analysis of steel frames equipped with NiTi shape memory alloy braces," *The Structural Design of Tall and Special Buildings*, vol. 23, no. 18, pp. 1406–1425, 2014.

[32] C. Qiu, Y. Zhang, H. Li, B. Qu, H. Hou, and L. Tian, "Seismic performance of concentrically braced frames with non-buckling braces: a comparative study," *Engineering Structures*, vol. 154, pp. 93–102, 2018.

[33] A. Rahman Bhuiyan and M. S. Alam, "Seismic performance assessment of highway bridges equipped with superelastic shape memory alloy-based laminated rubber isolation bearing," *Engineering Structures*, vol. 49, pp. 396–407, 2013.

[34] F. Hedayati Dezfuli and M. S. Alam, "Hysteresis model of shape memory alloy wire-based laminated rubber bearing under compression and unidirectional shear loadings," *Smart Materials and Structures*, vol. 24, no. 6, Article ID 065022, 2015.

[35] P. Sultana and M. A. Youssef, "Seismic performance of modular steel frames equipped with shape memory alloy braces," *Bulletin of Earthquake Engineering*, vol. 16, no. 11, pp. 5503–5527, 2018.

[36] F. Shi, O. E. Ozbulut, and Y. Zhou, "Influence of shape memory alloy brace design parameters on seismic performance of self-centering steel frame buildings," *Structural Control and Health Monitoring*, vol. 27, no. 1, Article ID e2462, 2020.

[37] H. Abou-Elfath, "Evaluating the ductility characteristics of self-centering buckling-restrained shape memory alloy braces," *Smart Materials and Structures*, vol. 26, no. 5, Article ID 055020, 2017.

[38] R. L. Boroschek, G. Farias, O. Moroni, and M. Sarrazin, "Effect of SMA braces in a steel frame building," *Journal of Earthquake Engineering*, vol. 11, no. 3, pp. 326–342, 2007.

[39] B. Andrawes and R. DesRoches, "Unseating prevention for multiple frame bridges using superelastic devices," *Smart Materials and Structures*, vol. 14, no. 3, pp. S60–S67, 2005.

[40] B. Andrawes and R. DesRoches, "Effect of ambient temperature on the hinge opening in bridges with shape memory alloy seismic restrainers," *Engineering Structures*, vol. 29, no. 9, pp. 2294–2301, 2007.

[41] H. Qian, H. Li, G. Song, and W. Guo, "Recentering shape memory alloy passive damper for structural vibration control," *Mathematical Problems in Engineering*, vol. 2013, Article ID 963530, 13 pages, 2013.

[42] H. S. Oliveira, A. S. De Paula, and M. A. Savi, "Dynamical jumps in a shape memory alloy oscillator," *Shock and Vibration*, vol. 2014, Article ID 656212, 10 pages, 2014.

[43] N. Mirzai and R. Attarnejad, "Seismic performance of EBFs equipped with an innovative shape memory alloy damper,"

*Scientia Iranica (Transactions A: Civil Engineering)*, vol. 27, no. 5, pp. 2316–2325, 2020.

[44] N. M. Mirzai, R. Attarnejad, and J. W. Hu, "Enhancing the seismic performance of EBFs with vertical shear link using a new self-centering damper," *International Journal*, vol. 35, pp. 57–75, 2018.

[45] N. M. Mirzai, R. Attarnejad, and J. W. Hu, "Analytical investigation of the behavior of a new smart recentering shear damper under cyclic loading," *Journal of Intelligent Material Systems and Structures*, vol. 31, no. 4, pp. 550–569, 2020.

[46] N. M. Mirzai and J. W. Hu, "Pilot study for investigating the inelastic response of a new axial smart damper combined with friction devices," *Steel and Composite Structures*, vol. 32, no. 3, pp. 373–388, 2019.

[47] H. Aryan and M. Ghassemieh, "Mitigation of vertical and horizontal seismic excitations on bridges utilizing shape memory alloy system," *Advanced Materials Research*, vol. 831, pp. 90–94, 2013.

[48] H. Aryan and M. Ghassemieh, "Seismic enhancement of multi-span continuous bridges subjected to three-directional excitations," *Smart Materials and Structures*, vol. 24, no. 4, Article ID 045030, 2015.

[49] H. Aryan and M. Ghassemieh, "A superelastic protective technique for mitigating the effects of vertical and horizontal seismic excitations on highway bridges," *Journal of Intelligent Material Systems and Structures*, vol. 28, no. 12, pp. 1533–1552, 2017.

[50] A. Abbass, R. Attarnejad, and M. Ghassemieh, "Seismic assessment of RC bridge columns retrofitted with near-surface mounted shape memory alloy technique," *Materials*, vol. 13, no. 7, p. 1701, 2020.

[51] M. A. Farmani and M. Ghassemieh, "Shape memory alloy-based moment connections with superior self-centering properties," *Smart Materials and Structures*, vol. 25, no. 7, Article ID 075028, 2016.

[52] M. A. Farmani and M. Ghassemieh, "Steel beam-to-column connections equipped with SMA tendons and energy dissipating devices including shear tabs or web hourglass pins," *Journal of Constructional Steel Research*, vol. 135, pp. 30–48, 2017.

[53] M. Ghassemieh, S. Mohyeddin Ghodratian, M. Reza Bahaari, and S. Ali Nojoumi, "Seismic enhancement of coupled shear walls using shape memory alloys," *Journal of Civil Engineering and Science*, vol. 2, no. 2, pp. 93–101, 2013.

[54] M. Ghassemieh, M. Mostafazadeh, and M. S. Sadeh, "Seismic control of concrete shear wall using shape memory alloys," *Journal of Intelligent Material Systems and Structures*, vol. 23, no. 5, pp. 535–543, 2012.

[55] M. Ghassemieh, M. Rezapour, and V. Sadeghi, "Effectiveness of the shape memory alloy reinforcement in concrete coupled shear walls," *Journal of Intelligent Material Systems and Structures*, vol. 28, no. 5, pp. 640–652, 2017.

[56] S. Hesami and V. Sadeghi, "Numerical investigation of the shape memory alloy dowels in jointed concrete pavements," *International Journal of Pavement Research and Technology*, vol. 8, no. 4, p. 251, 2015.

[57] M. S. Alam, M. A. R. Bhuiyan, and A. H. M. M. Billah, "Seismic fragility assessment of SMA-bar restrained multi-span continuous highway bridge isolated by different laminated rubber bearings in medium to strong seismic risk zones," *Bulletin of Earthquake Engineering*, vol. 10, no. 6, pp. 1885–1909, 2012.

[58] A. H. M. M. Billah, M. S. Alam, and M. A. R. Bhuiyan, "Fragility analysis of retrofitted multicolumn bridge bent subjected to near-fault and far-field ground motion," *Journal of Bridge Engineering*, vol. 18, no. 10, pp. 992–1004, 2013.

[59] F. H. Dezfuli and M. S. Alam, "Seismic vulnerability assessment of a steel-girder highway bridge equipped with different SMA wire-based smart elastomeric isolators," *Smart Materials and Structures*, vol. 25, no. 7, Article ID 075039, 2016.

[60] F. Hedayati Dezfuli, S. Li, M. S. Alam, and J.-Q. Wang, "Effect of constitutive models on the seismic response of an SMA-LRB isolated highway bridge," *Engineering Structures*, vol. 148, pp. 113–125, 2017.

[61] H.-L. Hsu, J.-L. Juang, and C.-H. Chou, "Experimental evaluation on the seismic performance of steel knee braced frame structures with energy dissipation mechanism," *Steel and Composite Structures*, vol. 11, no. 1, pp. 77–91, 2011.

[62] M. Mofid and P. Khosravi, "Non-linear analysis of disposable knee bracing," *Computers & Structures*, vol. 75, no. 1, pp. 65–72, 2000.

[63] M. Lotfollahi and M. Mofid, "On the design of new ductile knee bracing," *Journal of Constructional Steel Research*, vol. 62, no. 3, pp. 282–294, 2006.

[64] G. Aniello and G. Landolfo, "Seismic Response of Steel Frames with Knee Braces," in *Proceedings of the 7th European Conference On Steel And Composite Structures*, Naples, Italy, September 2014.

[65] I. Gholami Alam, M. Safi, and E. Darvishan, "Numerical and experimental performance evaluation of upgraded knee braces under cyclic load," *International Journal of Nonlinear Analysis and Applications*, vol. 13, no. 1, pp. 1863–1872, 2022.

[66] C. W. Roeder and E. P. Popov, "Eccentrically braced steel frames for earthquakes," *Journal of the Structural Division*, vol. 104, no. 3, pp. 391–412, 1978.

[67] L. Mastrandrea and V. Piluso, "Plastic design of eccentrically braced frames, I: moment–shear interaction," *Journal of Constructional Steel Research*, vol. 65, no. 5, pp. 1007–1014, 2009.

[68] H. Bahrampoor and G. S. Sabouri, "Effect of Easy-Going Steel Concept on the Behavior of diagonal Eccentrically Braced Frames," *International Journal of Civil Engineering*, vol. 8, 2010.

[69] A. Gholizad and P. Kamrani Moghaddam, "Friction damper dynamic performance in seismically excited knee braced steel frames," *International Journal of Civil Engineering*, vol. 12, no. 1, pp. 32–40, 2014.

[70] J. D. Aristizabal-Ochoa, "Disposable knee bracing: improvement in seismic design of steel frames," *Journal of Structural Engineering*, vol. 112, no. 7, pp. 1544–1552, 1986.

[71] M. Rezapour and M. Ghassemieh, "Macroscopic modelling of coupled concrete shear wall," *Engineering Structures*, vol. 169, pp. 37–54, 2018.

[72] R. DesRoches, J. McCormick, and M. Delemont, "Cyclic properties of superelastic shape memory alloy wires and bars," *Journal of Structural Engineering*, vol. 130, no. 1, pp. 38–46, 2004.

[73] H. Krawinkler, *ATC-24: Guidelines for Cyclic Seismic Testing of Components of Steel Structures*, Applied Technology Council, Redwood City, CA, USA, 1992.

[74] M. Ghassemieh, M. Rezapour, and A. Taghinia, "Predicting low cycle fatigue life through simulation of crack in cover plate welded beam to column connections," *Journal of Computational and Applied Mechanics*, vol. 48, no. 1, pp. 39–52, 2017.